Holographic Metasurface Based Modulation for Energy Efficient LEO Satellite Communication

Arumjeni Mitayani, Qingchao Li, *Graduate Student Member, IEEE,* Robert G. Maunder, *Senior Member, IEEE,* and Mohammed El-Hajjar, *Senior Member, IEEE*

***Abstract*—Non-Terrestrial Networks (NTN) have emerged as a key enabler for extending global connectivity, particularly in remote or infrastructure-limited regions. Given the stringent power constraints in satellite systems, especially in Low Earth Orbit (LEO) satellites, energy efficiency becomes a critical design requirement. In this paper, we propose a novel design for energy-efficient holographic metasurface-based modulation and beamforming for LEO satellite communication. Our approach employs a single radio frequency (RF) chain, significantly reducing power consumption compared to the conventional MIMO scheme while maintaining communication performance. To address the Lorentzian constraints inherent in holographic metasurfaces due to their magnetic polarizability, we introduce a beamforming strategy that effectively mitigates the impact of these physical limitations. Simulation results show that our proposed system achieves significant energy efficiency improvements over conventional fully digital and existing holographic beamforming architectures, with only a small trade-off in achievable data rate.**

***Index Terms*—Holographic metasurface, HMIMO, single RF chain, Lorentzian constraint, NTN, LEO satellite.**

I. Introduction

THE evolution of communication systems has always been driven by the constant demand for faster, more reliable, and efficient connectivity across various platforms [1]. As we transition from the era of the present 5G to the upcoming 6G communication systems, a significant leap in wireless technology is anticipated [2]. Traditional terrestrial network experiences difficulty to handle the surge of transmission demands by countless mobile devices and applications because of limited spectrum availability and restricted coverage [3]. Non-terrestrial networks (NTN) addresses these challenges with extending coverage, dynamic spectrum allocation, and employing beamforming [4]. On the other hand, NTNs have a restrictive link budget, high propagation delays, and different device capabilities [5]. Benefiting from lower latency transmission than the other satellite communication systems, low Earth orbit (LEO) satellites become ubiquitously used to provide terrestrial users with higher data rates [6]. Conventional MIMO has already been applied as a beamforming technique from satellite to the user [7]. On the other hand, conventional MIMO requires numerous radio frequency (RF) chains, which in satellite communication system has detrimental effect in power consumption and energy efficiency [8].

One promising approach that balances performance with energy efficiency is holographic MIMO (HMIMO), which offers transformative benefits for NTN systems [9]. HMIMO can improve the energy efficiency as well as support beamforming with a drastically reduced number of RF chains down to a single RF chain [10]. While this is a similar concept to analog beamforming, HMIMO structures do not require numerous phase shifters [9]. As a result, HMIMO achieves improved energy efficiency and simplified implementation, making it a compelling approach for NTN [11].

The implementation of HMIMO relies on using reconfigurable metasurfaces, which enable precise manipulation of electromagnetic waves [12]. These metasurfaces serve as the foundation for achieving efficient beamforming and reducing system complexity, enabling the development of modulation techniques that surpass traditional methods [13], [14]. Metasurface-based modulation differs fundamentally from spatial modulation and traditional antenna arrays in its approach to encoding information [15]. Spatial modulation encodes data by switching between active and inactive antennas, while metasurfaces manipulate electromagnetic waves directly through reconfigurable elements, eliminating the need for extra hardware [14]. This innovative approach eliminates the reliance on multiple RF chains, significantly reducing complexity and power consumption.

Holographic metasurfaces can be applied in LEO satellite communications due to their ability to form high-gain directional beams [16], compensating for significant free-space path loss at higher frequencies [17]. Unlike traditional phased arrays, which rely on power-intensive phase shifters, holographic metasurfaces use electromagnetic structures to control radiation patterns with lower power consumption and cost [18]. Their dynamic reconfigurability supports precise beam steering, crucial for maintaining reliable links amidst the high mobility of LEO satellites and ground terminals [19]. Additionally, they enable the use of larger radiation arrays without the complexity or expense of scaling phased-array systems.

More specifically, performance and analysis of holographic beamforming have been presented in [20]. Additionally, a technique known as wavenumber-division multiplexing was

The authors are with the School of Electronics and Computer Science, University of Southampton, Southampton SO17 1BJ, United Kingdom (email: A.Mitayani@soton.ac.uk; ql1d23@soton.ac.uk; rm@ecs.soton.ac.uk; meh@ecs.soton.ac.uk). Arumjeni Mitayani is also with the National Research and Innovation Agency (BRIN), Indonesia.

This work of Arumjeni Mitayani was supported by Indonesia Endowment Fund for Education (LPDP). Mohammed El-Hajjar would like to acknowledge the support of the Future Telecoms Research Hub, Platform for Driving Ultimate Connectivity (TITAN), sponsored by the Department of Science Innovation and Technology (DSIT) and the Engineering and Physical Sciences Research Council (EPSRC) under Grants EP/X04047X/1, EP/Y037243/1 and EP/X04047X/2.

TABLE I
CONTRIBUTIONS OF OUR PAPER COMPARED TO EXISTING RESEARCH

	Our Paper	[19]	[23]	[24]	[25]	[26]	[27]	[28]	[29]
Holographic MIMO	✓	✓	✓		✓	✓	✓	✓	
NTN Channel Model	✓	✓			✓	✓			
Lorentzian constraint	✓			✓			✓		
Single RF chain	✓		✓	✓					
No digital beamforming	✓		✓	✓					
Focus on energy efficiency	✓		✓	✓					✓
Holographic Metasurface Based Modulation	✓								

proposed in [21], which allows for low-complexity signal processing and interference mitigation by operating in the wavenumber domain. In contrast, there is also multi-user HMIMO scenarios [22], which helps in steering individual beams to different users in a downlink setup. It can create multiple beams with high accuracy and low sidelobe levels to serve multiple users with reduced interference.

Additionally, the earliest known holographic metasurface is reconfigurable holographic metamaterial antennas (RHMA) [30], which uses leaky-wave principle with recording and reconstruction process [31]. Although the purpose of RHMA has been applied for satellite communication, this model is preliminary and only focuses on sidelobe cancellation for the propagation. Afterwards, reconfigurable holographic surfaces (RHS) [32] based on the same principle with RHMA has been proposed. However, this architecture still requires hybrid beamforming method, where the digital beamforming is performed in the base station (BS). The effort to reduce the power consumption in the holographic metasurface is realized by reconfigurable refractive surface (RRS) [23]. RRS uses single feed and places the surface in the near-field regime of the feed. This model also has similarity with the dynamic metasurface antenna (DMA) [33], where metasurface consists of microstrips and each microstrip corresponds to the number of subelements.

The application of HMIMO systems to NTNs remains limited in several critical aspects [9]. Most existing works either overlook the physical constraints of metasurfaces, such as the Lorentzian constraint [19], or rely on energy-intensive digital beamforming architectures with multiple RF chains [23], which are impractical for energy-constrained satellite platforms. Additionally, only a few studies combine realistic NTN channel models with HMIMO design, and even fewer make energy efficiency a primary design objective. These shortcomings underscore the need for practical and efficient HMIMO solutions tailored to LEO satellite communication.

Several recent works, including [19], [23], and [25], have begun to incorporate HMIMO concepts in NTN contexts, with [19] and [25] considering NTN channel modeling. However, these often assume idealized metasurface behavior or ignore crucial physical constraints like the Lorentzian constraint, which plays a significant role in real-world implementations. In some prior works, the amplitude-phase trade-offs inherited by Lorentzian constraint have been directly applied in the system design without any mitigation [27], [28], while the latest research addresses phase compensation methods for handling the Lorentzian constraint [24], [34]. Although some efforts, such as [23] and [24], adopt single RF chain architectures to improve energy efficiency, [23] does not account for the Lorentzian constraint, thereby limiting the practical feasibility of their beamforming strategies, while [24] has individual power amplifier for each surface element. Conversely, works in [26] and [27] model the Lorentzian constraint but do not focus on NTNs or energy-efficient system design. To address these gaps, we propose a novel HMIMO system for LEO satellites that integrates holographic metasurface-based modulation and precoding under realistic hardware constraints. Our design includes the Lorentzian constraint and achieves energy-efficient transmission using a single RF chain. To the best of our knowledge, this is the first such integrated approach for NTN systems, and a detailed comparison of our contributions against the state-of-the-art is provided in Table I.

Hence, in this paper, we propose a holographic metasurface-based modulation and precoding technique designed for LEO satellite systems, which achieves high energy efficiency by utilizing a single RF chain. Our approach not only incorporates the Lorentzian constraint inherent to physical metasurfaces but also avoids digital beamforming on the satellite side, significantly reducing power consumption without compromising performance. While most existing methods rely on digital beamforming that demands multiple RF chains, our approach eliminates this need, offering a lightweight and efficient alternative. Our numerical results demonstrate higher energy efficiency compared to the state-of-the-art methods. Explicitly, our novel contributions can be summarized as follows:

- We design a holographic metasurface based modulation and precoding scheme, that requires a single RF chain for LEO satellite communications, where the holographic metasurface is placed on the satellite for communications with ground users.
- Our design incorporates a single RF chain aided feed that transmits an unmodulated signal to the metasurface, where the single-user signal is precoded and modulated on the metasurface. Here, a single RF chain radiates unmodulated signal to the holographic metasurface. The modulation and precoding is governed by the control module that is connected separately to the surface. In our proposed structure, a single power amplifier is embedded in the RF chain and amplifies the unmodulated signal.
- Our work adopts a realistic NTN channel model based on the 3GPP standard [35], providing a practical and accurate approximation for real-world applications.
- As the proposed method avoids digital processing, it significantly reduces power consumption, making it highly

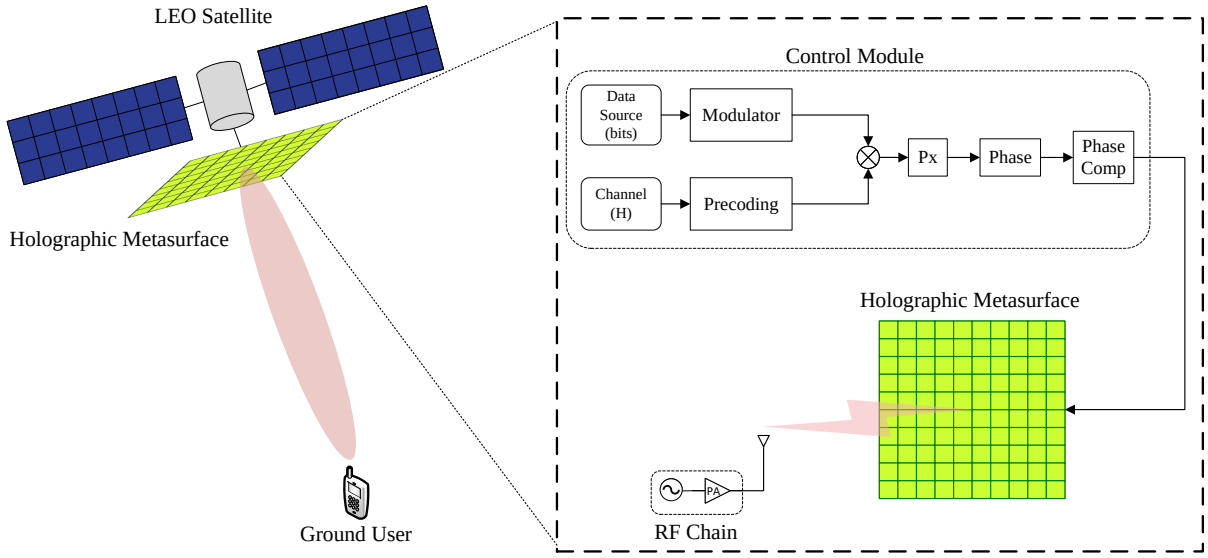

Fig. 1. Holographic Metasurface Based Modulation Architecture.

efficient for NTN communication systems. Our simulation results show an improvement of almost 1.5 bits/Joule/Hz from the existing structure of holographic MIMO and almost 2.5 bits/Joule/Hz from the fully digital architecture.

The rest of paper is organized as follows. In Section II, we introduce our system model, which is holographic metasurface based modulation that is equipped in a LEO satellite. In Section III, we discuss our simulation setup, e.g. NTN channel model that we use and performance metrics analysis. In Section IV, we provide the results and analysis. Finally, we draw conclusions in Section V.

Notations: The operation of transpose, conjugate, and Hermitian conjugate are represented by $(.)^{\top}$, $(.)^{*}$, and $(.)^{\mathsf{H}}$, respectively; $\otimes$ is the Kronecker product operation; $|a|$ and $\angle a$ denotes the amplitude and angle of the complex scalar a; $\|\mathbf{a}\|$ denotes the Euclidean norm of vector $\mathbf{a}$; a_n is the nth element of vector $\mathbf{a}$; $\mathcal{CN}(0,\sigma^2)$ is circularly symmetric complex Gaussian random number with mean 0 and variance σ^2.

II. System Model

Fig. 1 shows our proposed system model, where we consider a LEO satellite as a BS equipped with a holographic metasurface that acts as the signal transmitter, communicating with a ground user. The communication is in the downlink direction, from the satellite to the ground terminal. The satellite based holographic metasurface consists of multiple antenna elements that creates beamforming according to the holographic principle. The LEO satellite and ground user communicate over the NTN channel, which is explained in more detail in Subsection III-A. Since the communication between the LEO satellite's holographic metasurface and the ground user is using power that is allocated by the LEO satellite to the communication modules and is also limited, it becomes essential to design communication systems that have low power consumption and are cost-effective, hence a single RF chain analog processing is considered.

Our system is depicted in Fig. 1, where an unmodulated carrier signal is first generated by an oscillator, amplified via a power amplifier, and then radiated toward the holographic metasurface. Unlike conventional MIMO systems, where both modulation and power are delivered to the antenna array through the same RF signals, our architecture separates these two functions. The metasurface modulates the signal, using a predetermined modulation and precoding matrices, whilst also considering the Lorentzian constraint. The precoding and modulation are passed to the metasurface using the control module, as shown in Fig. 1. Since the Lorentzian constraint scales down the amplitude of the precoding weights, a capacity loss is inevitable in this structure. Hence, we propose a phase compensation technique to optimize the performance in Section II-C. The function of modulation and precoding is regulated by the digital processing module of the metasurface that is independent from the single RF chain used to feed the metasurface. Using this modulation and precoding, the transmitted signal constructively interferes in the desired direction, creating a beamforming towards the ground user. Each component of our proposed method is discussed in more details as follows.

A. Holographic Metasurface Based Modulation

In this paper, the LEO satellite's holographic metasurface acts as a transmitter and consists of $N \triangleq N_x \times N_y$ number of elements. The metasurface receives an unmodulated signal from the single RF chain feed source over the wireless channel as seen in Fig. 1. These metasurface elements capture the signals from the feed, modulate it using the surface elements and then transmit it to the ground user. The output from each element is determined by the signal processing module that directly controls the metasurface [36]. While conventional terminology may refer to control over both amplitude and

phase, in our system the surface elements directly control only the phase of the incident signal. However, due to the Lorentzian constraint, the phase modulation inherently affects the amplitude as well. This relationship constrains the achievable complex-valued beamforming weights and should be considered during system design. The control signal sets the real-valued phase shifts across the surface, which modulate the incident wave and enable beam steering toward the ground user. This control is realized by tuning the resonance characteristics of each metasurface element to implement the desired beamforming weights under the physical hardware constraints.

The metamaterial elements of the holographic metasurface function can be considered as resonant electrical circuits, with their frequency responses typically modeled as weights, where amplitude and phase are inherently linked by the Lorentzian constraint [24]. This constraint, denoted as $\mathcal{Q}$, is given by [37]

$$\mathcal{Q} = \frac{j + e^{j\phi}}{2}, \tag{1}$$

where ϕ represents the phase control signal, measured in radians, and $\mathcal{Q}$ is the output complex-valued IQ signal.

Originating from the physical structure of the holographic metasurface, the Lorentzian constraint plays a crucial role in beamforming performance and must be accounted for in system analysis. The following subsections provide a detailed discussion of the channel model and the impact of the Lorentzian constraint on beamforming design.

B. Proposed Holographic Metasurface Based Modulation and Beamforming Design

In this paper, we propose a holographic signal modulation that is integrated in the metasurface fed by single RF chain to beam signals to a single user. The data is processed in the digital processor, which forms the control unit that is connected to the holographic metasurface. The processing includes the modulation and precoding, which is separate from the RF chain. The phase of the unmodulated signal that is transmitted by the RF chain changes in the metasurface based on the controller. The physical system of the metasurface follows the concept of the Lorentzian constraint [26].

Conventionally, in a MIMO system, the data bits are modulated into a symbol vector x, which is then precoded using a precoding matrix $\mathbf{P}$, resulting in $\mathbf{P}x$. When applied to holographic metasurface, this signal is then passed through the physical metasurface response $\mathbf{Q}(\cdot)$, producing the final transmitted signal $\mathbf{Q}(\mathbf{P}x)$. In our system, the modulation and precoding are jointly applied in the control unit, and the metasurface acts on the already precoded signal, giving the final output

$$\mathbf{f}_{\text{HM}} = \mathbf{Q}(\mathbf{P}x), \tag{2}$$

where $\mathbf{Q}(\cdot)$ is the function of Lorentzian constraint, $\mathbf{P}x \in \mathbb{C}^{N\times 1}$ is the precoded signal, and $\mathbf{f}_{HM} \in \mathbb{C}^{N\times 1}$ is the vector of holographic modulated signal. Due to the Lorentzian constraint, achieving independent control over both amplitude and phase modulation is not feasible. This limitation prevents the implementation of unit amplitude modulation.

For example, consider the bit sequence `0011`, which is modulated using QPSK, where `00` maps to $\frac{1}{\sqrt{2}}(-1-j)$ and `11` maps to $\frac{1}{\sqrt{2}}(1+j)$. Each QPSK symbol is processed independently in time, so we define $\mathrm{x} \in \mathbb{C}$ as a scalar symbol selected from the QPSK-modulated symbol sequence at a given time instant. Suppose the metasurface consists of two elements, and we apply a vector precoder $\mathbf{P} = [1 + 0.5j,\ 0.5 + j]^\top \in \mathbb{C}^{2\times 1}$. For the first symbol $\mathrm{x} = \frac{1}{\sqrt{2}}(-1 - j)$, the precoded signal becomes $\mathbf{P}\mathrm{x} = \left[(1 + 0.5j)\frac{-1-j}{\sqrt{2}},\ (0.5 + j)\frac{-1-j}{\sqrt{2}}\right]^\top = \left[\frac{-0.5-1.5j}{\sqrt{2}},\ \frac{0.5-1.5j}{\sqrt{2}}\right]^\top$. This precoded signal is then passed through the metasurface response, giving $\mathbf{f}_{\text{HM}} = \mathbf{Q}(\mathbf{P}\mathrm{x})$, where $\mathbf{Q}(\cdot)$ denotes the Lorentzian-constrained mapping that adjusts the phase while changing the amplitude (e.g., to 0.5). For example, the element $\frac{1}{\sqrt{2}}(-0.5 - 1.5j)$ would be mapped to a Lorentzian-constrained equivalent $-0.1581 + 0.0257j$, where ϕ = -1.8925 is the original signal's phase. These constrained outputs are then applied to the holographic metasurface elements as phase shifts, enabling beam steering and modulation through surface-based signal processing.

Using this process, the control unit determines the necessary local resonance tuning (e.g., magnetic polarizability) to implement the complex-valued modulation $\mathbf{f}_{\text{HM}}$, ensuring that the resulting beam is steered in the desired direction with minimal power consumption, despite the physical constraints imposed by the metasurface.

Our proposed design works for any precoding methods, where we use the singular value decomposition as an example precoding in our analysis. The precoding vector of this system can be extracted from the right singular value of the channel $\mathbf{h}^\top \in \mathbb{C}^{1\times N}$ as follows

$$\mathbf{h}^\top = u \cdot \mathbf{\Sigma} \cdot \mathbf{v}^{\text{H}}, \tag{3}$$

where u is scalar value since we consider a single antenna ground user, $\mathbf{\Sigma}$ is $\mathbb{C}^{1\times N_x N_y}$, and $\mathbf{v}^{\text{H}} \in \mathbb{C}^{N_x N_y \times N_x N_y}$. Hence, we can write $\mathbf{P}$ as

$$\mathbf{P} = \mathbf{v}(:, 1). \tag{4}$$

Since the modulation of signal x is integrated in the holographic surface, the value of $\mathbf{f}_{\text{HM}}$ is restricted to the Lorentzian constraint of function $\mathbf{Q}(\cdot)$. It is intractable to make the solution of this problem analytical. Therefore, to simplify this holographic modulation system, we extract the phase of the right singular matrix in (4), multiply it by x, and apply it to the function of the Lorentzian constraint.

The Lorentzian constraint restricts the possible combinations of phase and amplitude for beamforming weights, posing a fundamental challenge in holographic metasurface design, where precise control over these parameters is essential. As a result, beamforming algorithms must account for this constraint to ensure that the calculated phase and amplitude settings are physically realizable by the metasurface. The constraint changes the original amplitude and phase into Lorentzian-modulated values (with amplitude fixed at $\frac{1}{2}$ and a scaled phase), which can result in infeasible values for $\mathbf{f}_{\text{HM}}$, particularly when the elements of $\mathbf{v}(1, :)$ are not confined to specific ranges.

The signal received by the ground user is denoted as y, represented as

$$y = \mathbf{h}^\top \mathbf{f}_{\text{HM}} + n, \tag{5}$$

where $\mathbf{h} \in \mathbb{C}^{N\times 1}$ is the channel between the holographic metasurface and the ground user and $\mathbf{n}$ is the noise within the propagation, with $n \sim \mathcal{CN}(0, \sigma^2)$.

It is worth noting that our proposed holographic metasurface based modulation and beamforming system is represented in similar modeling approach by [24], where it has been shown to provide accurate system-level insights. Although this approximation has not reflected hardware-specific nonlinearities, such as amplitude–phase coupling, the subsequent analysis remains valid for LEO satellite communication model. In Section IV, we further evaluate our scheme under Lorentzian-constrained conditions to demonstrate that our proposed method outperforms the benchmarkers for the energy efficiency.

C. Phase Compensation

Given the challenge of the Lorentzian constraint, we aim to maximize the selection of the phase in the holographic metasurface scenario, where we apply a phase compensation method [34] to our system. Specifically, we use maximum ratio (MR) principle to evaluate the phase compensation. Let us consider transmitting a signal $\mathbf{f}_{\text{MR}}$, which is used to calculate the optimum phase needed to maximize the signal's magnitude. In this case $\mathbf{f}_{\text{MR}}$ is restricted by the Lorentzian constraint, so that we have

$$\mathbf{f}_{\text{MR}} = \begin{bmatrix} \frac{j+e^{j\phi_1}}{2} \\ \frac{j+e^{j\phi_2}}{2} \\ \vdots \\ \frac{j+e^{j\phi_N}}{2} \end{bmatrix}, \tag{6}$$

where ϕ_n, $n = 1, \ldots, N$, denotes the phase of the n-th element in the holographic metasurface. We aim to maximize the value of $\left|\mathbf{h}^\top \mathbf{f}_{\text{MR}}\right|^2$ as

$$\begin{aligned} \max_{\phi_1,\phi_2,\ldots,\phi_N} \quad & \left|\mathbf{h}^\top \mathbf{f}_{\text{MR}}\right|^2 \\ \text{s.t.} \quad & \phi_n \in [0, 2\pi),\ \forall n = 1, \ldots, N, \\ & \left\|\mathbf{f}_{\text{MR}}\right\|^2 \le P_{\max}, \end{aligned} \tag{7}$$

where P_{max} is the maximum transmit power. Eventually, the maximum value for $\mathbf{f}_{\text{MR}}$ (constructed by $\phi_1, \phi_2, \ldots, \phi_N$), which is $\mathbf{f}^\star_{\text{MR}}$ can be summarized compactly by defining a transformation operator $\mathcal{Q}(\cdot)$:

$$\mathbf{f}^\star_{\text{MR}} = \mathcal{Q}(\mathbf{h}; \theta) \triangleq \frac{j + e^{j(\angle \mathbf{h}^* + \theta)}}{2}, \tag{8}$$

where θ equals to $\angle\left(\sum_{n=1}^N h_n\right) + \frac{\pi}{2}$.

Proof: In the following we prove (8) using two methods. First, we substitute the value of θ in $\mathbf{f}^\star_{\text{MR}}$ and derive $\mathbf{h}^\top \mathbf{f}^\star_{\text{MR}}$ to validate the maximum achievable result. In the second method, we show how to obtain θ that maximizes (8) starting with $\mathbf{h}^\top \mathbf{f}_{\text{MR}}$.

1) Let $c = \angle\left(\sum_{n=1}^N h_n\right)$, then $\theta = c + \frac{\pi}{2}$ and we can write $\mathbf{h}^\top \mathbf{f}^\star_{\text{MR}}$ as:

$$\begin{aligned} \mathbf{h}^\top \mathbf{f}^\star_{\text{MR}} &= \mathbf{h}^\top \left(\frac{j + e^{j(\angle \mathbf{h}^* + c + \frac{\pi}{2})}}{2}\right) \\ &= \sum_{n=1}^N h_n \frac{j + e^{j(\angle h_n^* + c + \frac{\pi}{2})}}{2} \\ &= \frac{j}{2}\sum_{n=1}^N h_n \ + \ \frac{1}{2}\sum_{n=1}^N h_n e^{j(\angle h_n^* + c + \frac{\pi}{2})} \\ &= \frac{j}{2}\sum_{n=1}^N h_n \ + \ \frac{1}{2}\sum_{n=1}^N h_n e^{j\angle h_n^*} e^{jc} e^{j\frac{\pi}{2}}. \end{aligned} \tag{9}$$

Since $e^{j\frac{\pi}{2}} = j$ and $|h_n| = h_n e^{j\angle h_n^*}$, we get

$$\mathbf{h}^\top \mathbf{f}^\star_{\text{MR}} = \frac{j}{2}\sum_{n=1}^N h_n \ + \ \frac{j}{2}\sum_{n=1}^N |h_n| e^{jc}. \tag{10}$$

Extracting the angle of both terms $\frac{j}{2}\sum_{n=1}^N h_n$ and $\frac{j}{2}\sum_{n=1}^N |h_n| e^{jc}$, we get

$$\angle\left(\frac{j}{2}\sum_{n=1}^N h_n\right) = \angle\left(\sum_{n=1}^N h_n\right) + \frac{\pi}{2}, \tag{11}$$

and since $|h_n|$ is a real number, it does not contain any phase. Then, we substitute back the $c = \angle\sum_{n=1}^N h_n$, we obtain

$$\begin{aligned} \angle\left(\frac{j}{2}\sum_{n=1}^N |h_n| e^{jc}\right) &= c + \frac{\pi}{2} \\ &= \angle\left(\sum_{n=1}^N h_n\right) + \frac{\pi}{2}. \end{aligned} \tag{12}$$

Because (11) is equivalent to (12), we guarantee that both vectors in (10) align and achieve their maximum value.

2) We can find the value of $\phi_1, \phi_2, \ldots, \phi_N$ by mathematical derivation of (7). We first set the initial value of $\mathbf{f}_{\text{MR}} = \mathcal{Q}(\mathbf{h}^*)$, so that $\mathbf{f}_{\text{MR}} = \left[\frac{j+e^{\angle h_1^*}}{2}, \frac{j+e^{\angle h_2^*}}{2}, \ldots, \frac{j+e^{\angle h_N^*}}{2}\right]^\top$. Hence, we get

$$\begin{aligned} \mathbf{h}^\top \mathbf{f}_{\text{MR}} &= \sum_{n=1}^N h_n \frac{j + e^{j\angle h_n^*}}{2} \\ &= \frac{j}{2}\sum_{n=1}^N h_n \ + \ \frac{1}{2}\sum_{n=1}^N h_n e^{j\angle h_n^*}. \end{aligned} \tag{13}$$

In this case, each channel coefficient can be written as $h_n = |h_n| e^{j\angle h_n}$, so that the magnitude is equivalently expressed as $|h_n| = h_n e^{-j\angle h_n} = h_n e^{j\angle h_n^*}$, for $n = 1, \ldots, N$. Then, we can substitute (13) as

$$\mathbf{h}^\top \mathbf{f}_{\text{MR}} = \frac{j}{2}\sum_{n=1}^N h_n \ + \ \frac{1}{2}\sum_{n=1}^N |h_n|. \tag{14}$$

In (14), the term $\frac{1}{2}\sum_{n=1}^N |h_n|$ is purely real and lies along the positive x-axis, while the term $\frac{j}{2}\sum_{n=1}^N h_n$ is complex. To maximize the magnitude of the sum in (14), we need to align

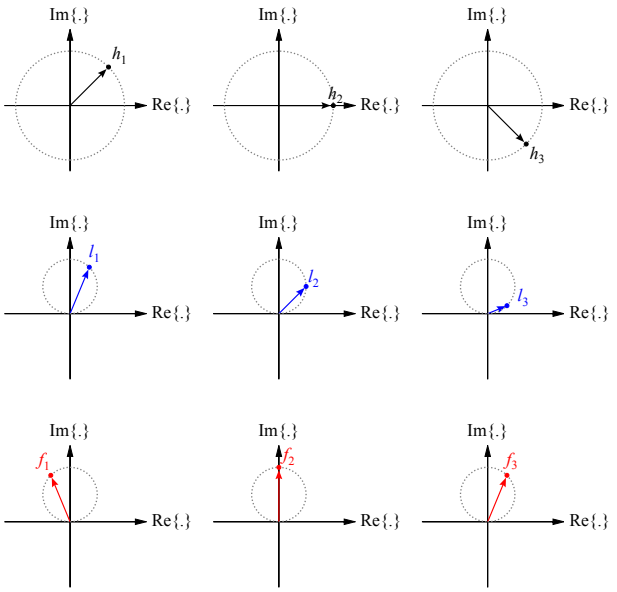

Fig. 2. Lorentzian transformation of vectors and phase compensation.

these two vectors such that their phasors add constructively. Geometrically, we can represent (14) as the vector sum of two components separated by an angle θ. The optimal alignment is achieved by adjusting the phases of the metasurface elements to compensate for this separation, resulting in

$$\begin{aligned}\theta &= \angle\left(\frac{j}{2}\sum_{n=1}^{N} h_n\right)\\ &= \angle\left(\frac{1}{2}\sum_{n=1}^{N} h_n\, e^{j\frac{\pi}{2}}\right)\\ &= \angle\left(\sum_{n=1}^{N} h_n\right)+\frac{\pi}{2}.\end{aligned} \tag{15}$$

Therefore, the values of $\phi_1, \phi_2, \ldots, \phi_N$ that obtain the maximum value for $\mathbf{hf}_{\mathrm{MR}}$ is $\phi_n = \angle h_n^* + \theta$, for $n = 1, 2, \ldots, N$, which proves (8). This representation makes clear that the Lorentzian constraint inherently enforces a $\pi/2$ phase rotation, and the optimal phase compensation aligns the controllable term accordingly to maximize (7).

Fig. 2 is the illustration of the phase compensation in the Lorentzian constrained weights. The first row denoted by h_1, h_2, and h_3 is the original normalized weights with unit magnitude. Then, we extract the phase and apply it in the Lorentzian form as seen in the second row of Fig. 2, which is l_1, l_2, and l_3. It can be seen that if, for example, we have $h_1 = e^{j\phi_1}$, then we have $l_1 = \frac{j+e^{j\phi_1}}{2}$. The last row of Fig. 2 is the weights after the phase compensation, which are denoted by f_1, f_2, and f_3.

Without loss of generality, the top subfigures of Fig. 2 show the unconstrained beamforming vectors of $\mathbf{P}x$. Let us consider an example with $h_1 = e^{j\pi/4}$, $h_2 = e^{j0}$, and $h_3 = e^{j-\pi/4}$. The figures in the second row of Fig. 2 are when the phase of the unconstrained beamforming vectors is applied directly to the Lorentzian function (1), so that $l_1 = \frac{j+e^{j\pi/4}}{2}$ and the same thing happens to l_2 and l_3. We can see that the top subfigures are scaled in such a way that they construct half magnitude vectors shown in the second row of Fig. 2. The third row of Fig. 2 represents the beamforming vectors after applying the proposed phase compensation. For instance, after the calculation of the vector in (15), we find the phase compensation θ to apply in (8). With the selection of $\mathbf{h}$ in Fig. 2, the calculated θ is $\frac{\pi}{2}$, so that $f_1 = \frac{j+e^{j(\pi/4+\pi/2)}}{2}$. In Fig. 2, f_1, f_2 and f_3 are 90° rotation from l_1, l_2, and l_3, respectively. The phase rotation may vary with the other values of $\mathbf{h}$ according to (15).

III. Simulation Setup

In this paper, to have realistic performance results, we apply the 3GPP NTN channel model in our simulations. We evaluate the system performance by analyzing the capacity as a function of the number of holographic metasurface elements. Subsequently, we calculate the power consumption of our proposed method, and compare with the existing DMA structure as well as the fully digital architecture. From these metrics, we can compute the energy efficiency for each method and compare them in the same simulation environment. We also evaluate the simulation results, when considering single and multiple streams communication to a single antenna user.

A. NTN Channel Model

In our simulations, the 3GPP NTN channel model [35] is considered for the link between the holographic metasurface with the user u located at the ground [38]. The metasurface in the satellite is considered in the xy-axis and the z-axis refers to the vertical direction to the Earth. For more realistic channel model, we also incorporate channel parameters for NTN suggested by [35]. Here, NTN communication channel adopts tapped delay line (TDL) model that has already been adjusted and measured for communication between satellite and ground user. It has two main models, which are line-of-sight (LOS) and non line-of-sight (NLOS) schemes, each of which has different parameters. Here, we represent NTN-TDL-A channel as the LOS model and NTN-TDL-C channel as the NLOS model, where both models have different multipath delays. In [35], the values for multipath delays are limited to the elevation angle of 50° only.

Moreover, we adopt uniform rectangular planar array (URPA) [38] for our rectangular form holographic metasurface, which implements planar wave assumption. As seen in Fig. 1, the URPA model of the metasurface adhered to satellite considering xy-axis is described as

$$\begin{aligned}\mathbf{s}(\theta_u, \phi_u, r_u) &= \mathbf{a}_x(\theta_u, \phi_u) \otimes \mathbf{a}_y(\theta_u, \phi_u)\\ &= \frac{1}{\sqrt{N}}\Big[1, e^{j\frac{2\pi}{\lambda} d \sin\theta_u \cos\phi_u}, \ldots, e^{j\frac{2\pi}{\lambda}\ldots}\\ &\quad \ldots(N_x-1)d\sin\theta_u\cos\phi_u\Big] \otimes \Big[1, e^{j\frac{2\pi}{\lambda} d\sin\theta_u \ldots}\\ &\quad \ldots \sin\phi_u, \ldots, e^{j\frac{2\pi}{\lambda}(N_y-1)d\sin\theta_u\sin\phi_u}\Big],\end{aligned} \tag{16}$$

where $\mathbf{s}(\theta_u, \phi_u, r_u)$ denotes the location of the user, with θ_u, ϕ_u, and r_u being the elevation, azimuth, and radius of the user from the perspective of the satellite. Moreover, $\otimes$ is the Kronecker product which multiplies steering vector in the x-axis $\mathbf{a}_x(\theta_u, \phi_u)$ and steering vector in y-axis $\mathbf{a}_y(\theta_u, \phi_u)$ in element-wise manner as follows

$$\begin{aligned}\mathbf{a}_x(\theta_u, \phi_u) \otimes \mathbf{a}_y(\theta_u, \phi_u) = \Big[&\mathbf{a}_{x(1)}(\theta_u, \phi_u)\mathbf{a}_y(\theta_u, \phi_u),\\ &\mathbf{a}_{x(2)}(\theta_u, \phi_u)\mathbf{a}_y(\theta_u, \phi_u),\\ &\ldots,\\ &\mathbf{a}_{x(N_x)}(\theta_u, \phi_u)\mathbf{a}_y(\theta_u, \phi_u)\Big].\end{aligned} \tag{17}$$

Therefore, combining (16) and (17), we have

$$\begin{aligned}\mathbf{s}(\theta_u, \phi_u, r_u) = \frac{1}{\sqrt{N}}\Big[&1,\ e^{j\frac{2\pi}{\lambda}d\sin\theta_u\sin\phi_u}, \ldots,\\ &e^{j\frac{2\pi}{\lambda}d\sin\theta_u\cos\phi_u}, \ldots,\\ &e^{j\frac{2\pi}{\lambda}d\sin\theta_u\left((N_x-1)\cos\phi_u+(N_y-1)\sin\phi_u\right)}\Big].\end{aligned} \tag{18}$$

The corresponding row vector channel $\mathbf{h}^\top \in \mathbb{C}^{1\times N_x N_y}$ can be represented as [38]

$$\mathbf{h} = \sqrt{L}\,\mathbf{b}(\theta_u, \phi_u, r_u), \tag{19}$$

where L denotes the large-scale pathloss between the satellite and the user, while $\mathbf{b}(\theta_u, \phi_u, r_u) \in \mathbb{C}^{1\times N_x N_y}$ encapsulates the element-dependent small-scale channel gains. Specifically, the n-th entry of $\mathbf{b}(\theta_u, \phi_u, r_u)$ can be expressed as

$$b_n = \sqrt{\beta_n}\, s_n(\theta_u, \phi_u, r_u), \tag{20}$$

where β_n accounts for the element-specific gain incorporating spherical wavefront effects and atmospheric attenuation, which depends on carrier wavelength, rain attenuation coefficient, and antenna gain [39], while $s_n(\theta_u, \phi_u, r_u)$ denotes the propagation direction from the (n_x, n_y)-th element of the metasurface to the user.

B. Capacity

In this holographic metasurface based modulation, the continuous-input continuous-output memoryless channel (CCMC) capacity is defined as

$$\mathrm{C_{HM}} = \log_2\left(1 + \frac{P_t}{\sigma_n^2}\left|\mathbf{h}^\top \mathbf{f}_{\mathrm{MR}}\right|^2\right). \tag{21}$$

Our aim is to maximize the capacity, which is also reflected in maximizing the $\mathbf{h}^\top\mathbf{f}_{\mathrm{MR}}$ term in (7). Theoretically, using a single RF chain for modulation and precoding will possibly reduce the capacity compared to full RF chain utilized by the fully digital scheme. We aim to optimize the capacity of this single RF chain design as a means of minimizing the capacity loss from reducing the number of RF chain.

In the conventional phased antenna array, the distance between elements is usually $\frac{\lambda}{2}$, while holographic metasurface allows inter-elements distance $< \frac{\lambda}{2}$ [40]. This phenomenon will compensate the capacity loss due to the mutual coupling of elements in the holographic metasurface. The discrete-input continuous-output memoryless channel (DCMC) capacity of holographic metasurface system is given by [15].

C. Power Consumption

The power consumption of holographic metasurface aided communication system with a single RF chain can be calculated as [41]

$$\mathrm{P_{HM}} = \mathrm{P_T}/\kappa + \mu + 2\mathrm{P_{DAC}} + \mathrm{P_{RF}} + \eta\mathrm{C_{HM}}, \tag{22}$$

where $\mathrm{P_T}$, κ, μ, $\mathrm{P_{DAC}}$, $\mathrm{P_{RF}}$, η, and $\mathrm{C_{HM}}$ denote the transmit power radiated through the system, the power amplifier efficiency, the passive circuit power of the holographic metasurface, the digital-to-analog converter power, the RF chain power, the signal coding regulator, and capacity, respectively. In addition, the control unit of the holographic metasurface is included in the passive circuit power of the holographic metasurface[1] μ.

Generally, the link between the power amplifier as a part of RF chain and holographic metasurface can be modeled as near field channel. Since holographic metasurface is fully passive device, it does not consume power unlike the antenna array.

In this paper, we compare our system's performance with fully digital architecture and existing DMA methods. The digital architecture has a significantly different power consumption with our method. Meanwhile, the power consumption of existing DMA methods have similarity with our method's power consumption. For the existing DMA structure, the number of RF chain is the same with the number of microstrip, which is denoted by N_T^{RF}. The power consumption for the fully digital and the DMA architectures are, respectively, denoted as [42]

$$\mathrm{P_{FD}} = \mathrm{P_T}/\kappa + \mu + N_T\left(2\mathrm{P_{DAC}} + \mathrm{P_{RF}}\right) + \eta\mathrm{C_{FD}}, \tag{23}$$

$$\mathrm{P_{DMA}} = \mathrm{P_T}/\kappa + \mu + N_t^{RF}\left(2\mathrm{P_{DAC}} + \mathrm{P_{RF}}\right) + \eta\mathrm{C_{DMA}}. \tag{24}$$

The power consumption between fully digital system and the holographic metasurface based modulation can be differentiated by the number of RF chain as the multiplier for RF chain power P_{RF}. In our proposed holographic metasurface, the power consumption contributed by RF chain is low, since we use a single RF chain, while in the fully digital system, the number of transmit RF chain is the same as the number of transmit antennas.

As benchmarkers for power consumption, we consider the hybrid beamforming method for LEO satellite communication [43]–[45]. Here, we use fully connected and partially connected hybrid beamforming schemes, where the power consumption can be evaluated as [46]

$$\begin{aligned}\mathrm{P_{FCH}} = &\frac{\mathrm{P_T}}{\kappa} + \mu + N_t^{RF}\left(2\mathrm{P_{DAC}} + \mathrm{P_{RF}}\right)\\ &+ N_t N_t^{RF} P_{PS} + \eta\mathrm{C_{FCH}},\end{aligned} \tag{25}$$

$$\begin{aligned}\mathrm{P_{PCH}} = &\frac{\mathrm{P_T}}{\kappa} + \mu + N_t^{RF}\left(2\mathrm{P_{DAC}} + \mathrm{P_{RF}}\right)\\ &+ N_t^{RF} N_t^{RF} P_{PS} + \eta\mathrm{C_{FCH}},\end{aligned} \tag{26}$$

[1]The control unit power consumption is inherently included in (22), following the system-level modeling approach in [41].

where $\mathrm{P_{FCH}}$, $\mathrm{P_{PCH}}$, and $\mathrm{P_{PS}}$ denote power consumption of the fully connected hybrid architecture, the partially connected hybrid architecture, and the phase shifters, respectively.

D. Energy Efficiency

Energy efficiency is measured as the ratio of data capacity to power consumption, indicating the number of bits transmitted per Joule of energy. This metric is important for our system to evaluate the performance against the power constraint that exists in LEO satellite communication. The energy efficiency of holographic metasurface based modulation $\mathrm{EE_{HM}}$ is given by

$$\mathrm{EE_{HM}} = \frac{\mathrm{C_{HM}}}{\mathrm{P_{HM}}}. \tag{27}$$

We will compare the performance of energy efficiency for our proposed methods, fully digital scheme, and the existing DMA structure. We expect a higher energy efficiency for our method, since our method has significantly lower power consumption as the RF chain is reduced down to one.

For hybrid beamforming architectures, we use the upper bound capacity for energy efficiency analysis, which is the capacity of fully digital antenna. Therefore, the hybrid beamforming architectures' performance here is the best performance that can be achieved by the hybrid beamforming architectures.

E. Multiple Stream Analysis

In the multiple stream scenario, we consider multiple data streams transmitted simultaneously from the metasurface, where applying this using a single-RF chain presents a potential challenge. To ensure that our proposed system works in multiple data streams scenario, we implement multiple users with different channels. Then, the channels expands into a matrix $\mathbf{H}^{\top} \in \mathbb{C}^{M \times N_x N_y}$, with the SVD of $\mathbf{H}^{\top}$ defined as

$$\mathbf{H}^{\top} = \mathbf{U} \cdot \mathbf{\Sigma} \cdot \mathbf{V}^{\mathrm{H}}, \tag{28}$$

where $\mathbf{U}$ is an $(M \times M)$ matrix. We expand (4) into a multiple streams scenario as

$$\mathbf{Q}(\mathbf{P}) = \mathbf{V}(:, 1:M), \tag{29}$$

where M is the number of streams used in this system.

IV. Results and Discussions

In this section, we analyze the performance of our proposed technique and compare the results with some benchmark schemes, such as existing DMA structure and fully-digital scheme. In the following figures, we refer to our proposed method as Holo-MBM, which means holographic metasurface based modulation method. The DMA structure with MISO system presented in [24] is the most comparable system with our proposed method. Firstly, we analyze the capacity, where the fully digital scheme acts as the upper bound of the capacity calculation. Additionally, since our focus is on the energy efficiency, we present the energy efficiency of our proposed method.

TABLE II
Simulation Parameter

Passive Circuit Power: μ	0.1 W
RF Chain Power: P_{RF}	0.02 W
Phase Shifter Power: P_{PS}	0.0216 W
Power Amplifier Efficiency: κ	0.65
Transmit Power: P_T	0.125 – 8 W
Number of Metasurface Elements: N	56, 504
Number of Digital Antenna: N_T	28, 252
Number of RF Chains: N_{RF}	1 4, 18 56, 504

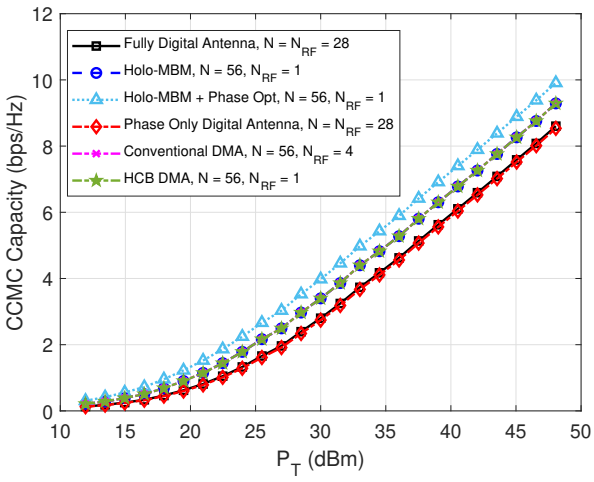

Fig. 3. Capacity comparison of our proposed method with the benchmarkers for N = 56.

In our simulations, we use $N = 56$ elements consisting of 4×14 holographic metasurface elements. Given the smaller distance between the metasurface elements compared to the phased antenna arrays, we use the number of elements in the holographic MIMO twice that of the fully digital schemes [24]. In the same surface area, the holographic metasurface has more elements than phased antenna array, since it is more dense and packed. The parameters used in the simulation are shown in Table II.

Fig. 3 shows the CCMC capacity of our proposed method compared to the existing methods, such as fully digital antenna array and multiple RF chain DMA with the number of antenna elements $N = 56$, where in the fully digital method, the number of antenna is $N = 28$. Additionally, Fig. 4 shows the result for $N = 504$. For the same number of antenna elements in the holographic metasurface and fully digital antenna array, the capacity loss caused by Lorentzian constraint is significant. Nevertheless, this is the physical constraint of holographic metasurface that cannot be avoided. However, compared to the structure having the same constraint but using multiple RF chains, the capacity loss is insignificant.

Fig. 5 shows the DCMC capacity for BPSK, QPSK, and 16-QAM. As given in the theory, our proposed method will reach the maximum of 1 bps/Hz, 2 bps/Hz, and 4 bps/Hz for BPSK, QPSK, and 16-QAM, respectively. Here, the DCMC capacity is shown to give a clearer visualization how quick each method

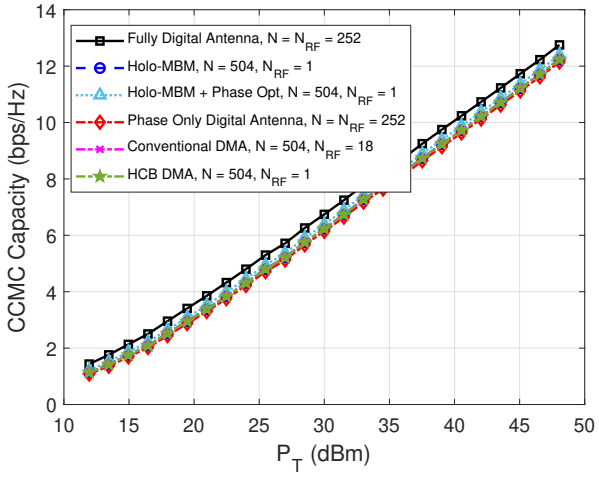

Fig. 4. Capacity comparison of our proposed method with the benchmarkers for N = 504.

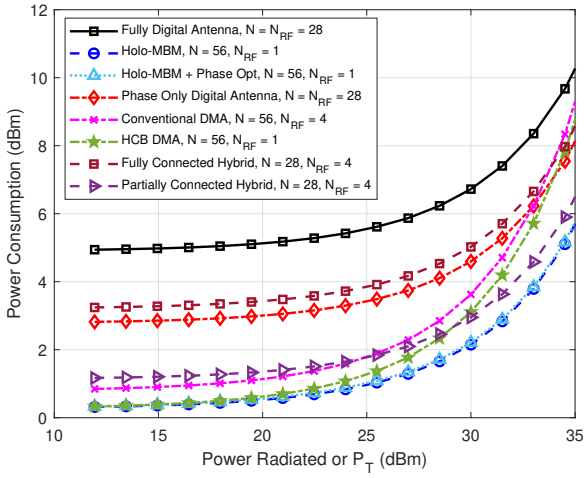

Fig. 6. Power consumption of the proposed holographic metasurface system compared to the benchmark methods.

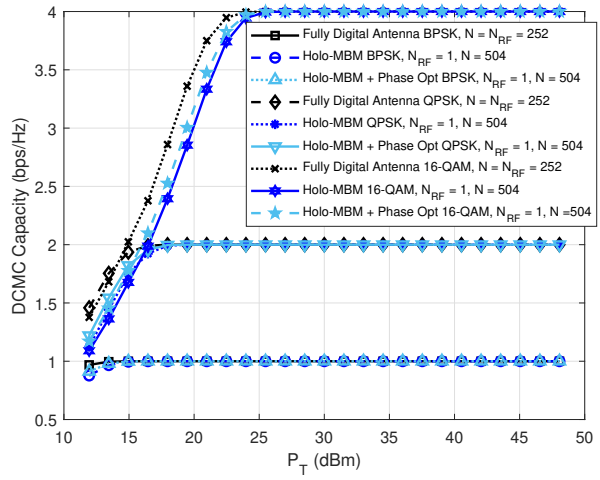

Fig. 5. Capacity comparison of our proposed method with the benchmarkers.

reaches the asymptotic value for each modulation.

Additionally, we analyze the power consumption of our proposed scheme and the existing methods. From Fig. 6, we can see that the power consumption of the fully digital antenna array is significantly larger than the other schemes, since the power for the digital beamformer is multiplied by the total number of antenna elements in the system. When the antenna array uses the larger number of antenna elements, the power consumption will also increase. Meanwhile, in our proposed scheme, the power consumption is low thanks to using only single RF chain and single power amplifier. In NTN, especially LEO satellite, having an energy efficient design is beneficial as the power source in the satellite is not abundant as it is in terrestrial network.

In Fig. 7 and Fig. 8, we show the simulation results for energy efficiency of our proposed method and the benchmark methods. Our proposed method with the phase enhancement has the best result, where it has highest energy efficiency in lower transmit power. There is a state when the capacity can no longer compensate for the power consumption, when the curve of the energy efficiency starts to decline. To reach the energy efficiency peak, our proposed method need a transmit power of 21 dBm, which is categorized as low and reasonable to put in the satellite. Meanwhile, the conventional DMA culminates in transmit power of 28 dBm with the same energy efficiency. The energy efficiency of the fully digital antenna array remains the worst as predicted, despite its high capacity. However, when we increase the number of elements as shown in Fig. 8, the peak is shifted to the left, which is to the lower transmit power, and the fully connected hybrid beamforming architecture has the worst performance because of much higher number of phase shifters according to (25). Meanwhile, for both numbers of antenna elements, the partially connected hybrid beamforming architecture has less energy efficiency than the conventional DMA with multiple RF chains, because in our simulations, both conventional DMA and partially connected hybrid beamforming have the same number of RF chains with the latter having more power consumption contribution from the phase shifters. However, conventional DMA still benefits from less power consumption of the metasurface. It means that with higher number of antenna elements, our proposed method needs lower transmit power to attain the highest energy efficiency.

To add more insight to our results, we also provide the power efficiency graph, defined as the ratio of the transmit power over power consumption, as seen in Fig. 9. As we define our power amplifier efficiency $\kappa = 0.65$, we expect to see that our proposed method has the best performance, which is proven in the figure. In the same radiated power P_T, our proposed method has the highest power efficiency, because there is only small loss from the other power contributing factors. Meanwhile, the main contributing factor in fully digital scheme's power consumption is not the power amplifier efficiency, but the power consumption of the RF chain. The existing DMA structure has lower power efficiency than our

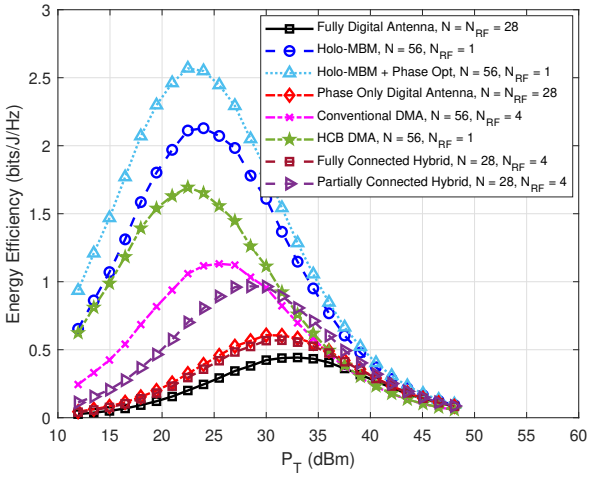

Fig. 7. Energy efficiency of the proposed holographic metasurface system compared to the benchmark methods, for N = 56.

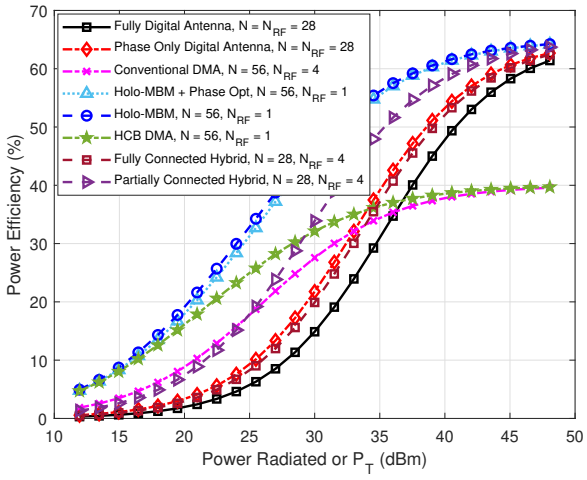

Fig. 9. Power efficiency of the proposed holographic metasurface system compared to the benchmark methods.

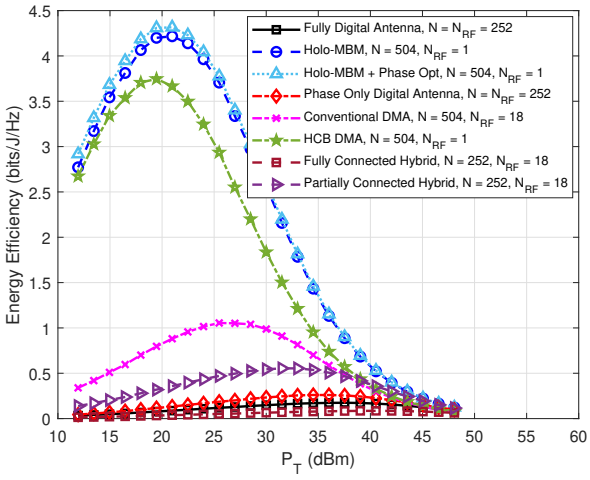

Fig. 8. Energy efficiency of the proposed holographic metasurface system compared to the benchmark methods, for N = 504.

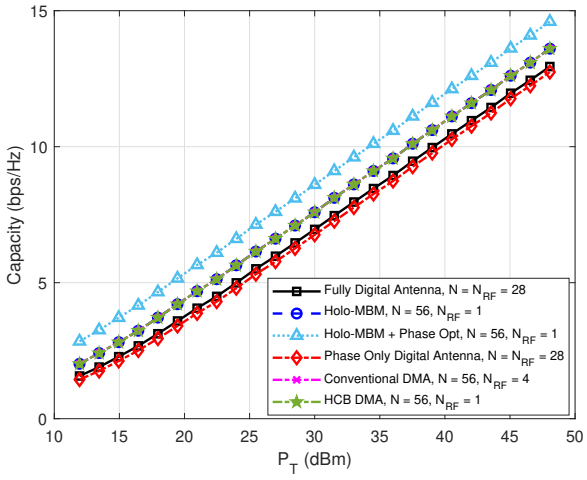

Fig. 10. Capacity comparison of our proposed method with the benchmarkers for N = 56 in NTN-TDL-C channel model.

proposed method, because it has significant loss in the power divider that is connected to each of the microstrip of the DMA, which affects the power amplifier efficiency. Meanwhile, the fully connected hybrid beamforming power efficiency has worse performance than that of partially connected hybrid beamforming, while it is still under our proposed method's performance.

We show the performance of LOS model, which is the NTN-TDL-C channel model defined by [35]. This channel model has different multipath delays than the NTN-TDL-A channel model. As seen in Fig. 10 and Fig. 11, the capacity increases drastically when using NTN-TDL-C channel model, which results in an improved energy efficiency. This is due to the higher beamforming gain in the LOS channel model.

Additionally, we present the results for multiple stream transmission based on the proposed holographic metasurface communication system, with the number of stream $M = 4$ and $M = 8$. In the NLOS channel model, which is the

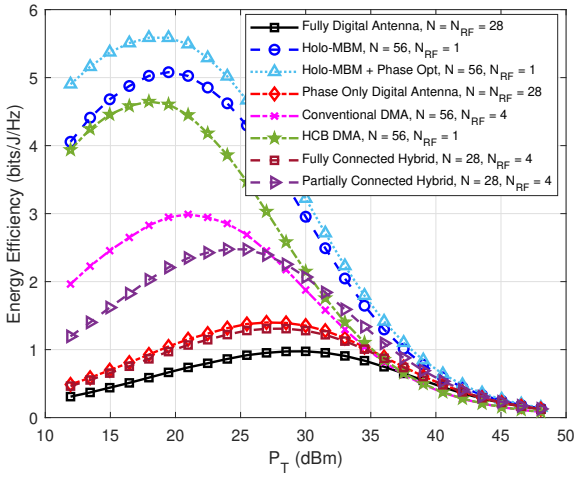

Fig. 11. Energy efficiency of the proposed holographic metasurface system compared to the benchmark methods, for N = 56 in NTN-TDL-C channel model.

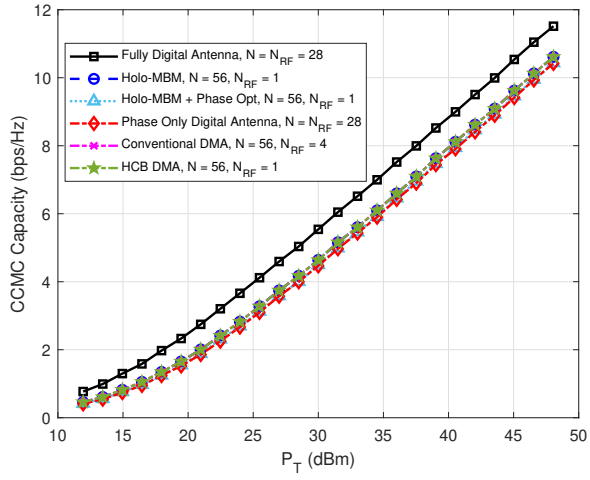

Fig. 12. Capacity of the holographic metasurface system compared with the benchmarkers for $M = 4$ streams.

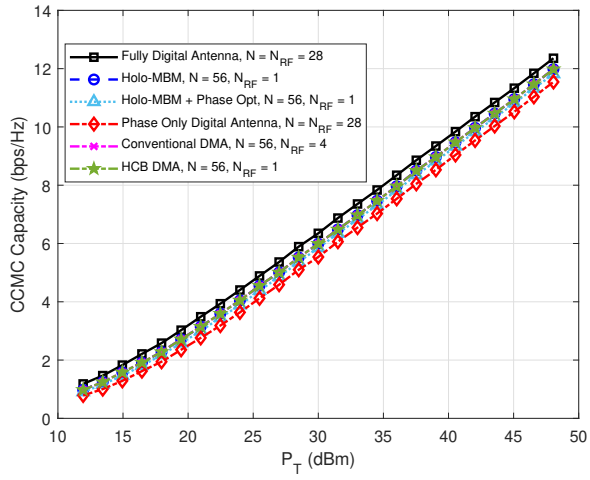

Fig. 13. Capacity of the holographic metasurface system compared with the benchmarkers for $M = 8$ streams.

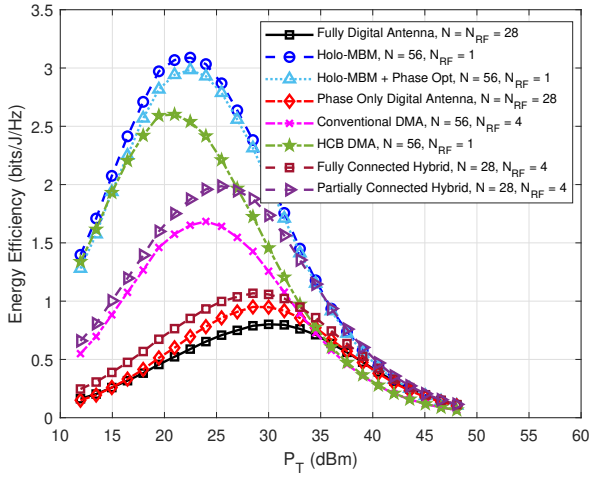

Fig. 14. Energy efficiency of the holographic metasurface system compared with the benchmarkers for $M = 4$ streams.

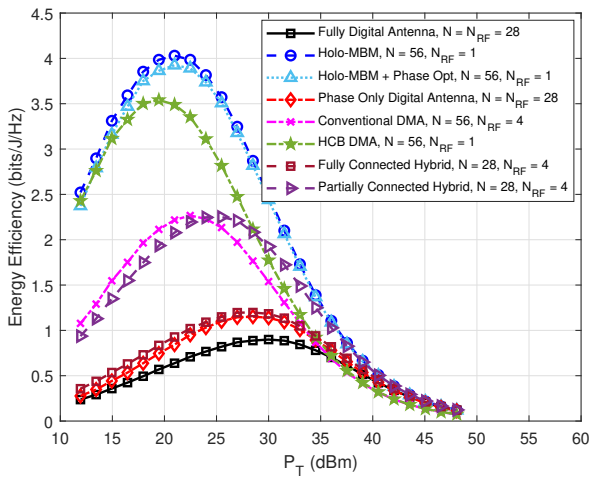

Fig. 15. Energy efficiency of the holographic metasurface system compared with the benchmarkers for $M = 8$ streams.

NTN-TDL-A channel model, increasing the number of streams can increase the capacity as seen in Fig. 12 and Fig. 13 with the assumption of ideal channel separation, with no inter-stream interference between the streams. Moreover, the energy efficiency for our proposed method increases by 1 bit/Joule/Hz if we increase the number of streams from 4 to 8 as shown in Fig. 14 and Fig. 15. Note that joint phase optimization is needed in multi-stream scenario to find the optimum phase compensation values. The results in Fig. 14 and Fig. 15 show the potential of applying our method in multiple stream scenarios, where we plan to design phase compensation techniques in multiple stream and multiple user scenarios, in our future work.

V. Conclusion and Future Work

In this paper, we proposed a holographic metasurface-based modulation and precoding scheme attached to a LEO satellite employing a single RF chain. The beamforming in the holographic metasurface was designed to reduce the capacity loss due to the physical structure limitation of the surface, i.e., the Lorentzian constraint. Since the LEO satellite communication system has stringent link budget requirements, we maximized the energy efficiency of our proposed method by optimizing the power consumption of the system. Applying a single RF chain in our system was shown to reduce power consumption significantly. The results show that holographic metasurface-based modulation can increase the energy efficiency compared to the existing structure of holographic beamforming and conventional fully digital phased-array antennas.

For future work, we plan to extend this framework to multi-stream and multi-user scenarios. In Section IV, we presented preliminary results for multi-stream scenarios. These results show that increasing the number of streams can increase system capacity under the NTN channel model, assuming ideal channel separation. Using our proposed method, energy efficiency also improves by approximately 1 bit/Joule/Hz when scaling from 4 to 8 streams. However, we note that in realistic scenarios, inter-stream interference will require a

careful design. Therefore, in future work we will develop joint phase optimization techniques under the Lorentzian constraint to mitigate inter-stream interference, enabling practical deployment of multi-stream transmission. We expect this extension to significantly enhance both capacity and energy efficiency in holographic metasurface based modulation and beamforming in NTN systems. In addition, our future work will address multiple-user NTN scenarios, including the minimum number of RF chains required to support M users, the number of users a single RF chain can serve with acceptable performance degradation, and the impact of the Lorentzian constraint on inter-user interference.

REFERENCES

[1] M. Attaran, "The impact of 5G on the evolution of intelligent automation and industry digitization," *Journal of Ambient Intelligence and Humanized Computing*, vol. 14, pp. 5977–5993, 2023.

[2] W. Chen, X. Lin, J. Lee, A. Toskala, S. Sun, C. F. Chiasserini, and L. Liu, "5G-Advanced Toward 6G: Past, Present, and Future," *IEEE Journal on Selected Areas in Communications*, vol. 41, no. 6, pp. 1592–1619, 2023.

[3] C. Niephaus, M. Kretschmer, and G. Ghinea, "QoS Provisioning in Converged Satellite and Terrestrial Networks: A Survey of the State-of-the-Art," *IEEE Communications Surveys & Tutorials*, vol. 18, no. 4, pp. 2415–2441, 2016.

[4] A. Guidotti, A. Vanelli-Coralli, and C. Amatetti, "Federated Cell-Free MIMO in Nonterrestrial Networks: Architectures and Performance," *IEEE Transactions on Aerospace and Electronic Systems*, vol. 60, no. 3, pp. 3319–3347, 2024.

[5] M. Hosseinian, J. P. Choi, S.-H. Chang, and J. Lee, "Review of 5G NTN Standards Development and Technical Challenges for Satellite Integration With the 5G Network," *IEEE Aerospace and Electronic Systems Magazine*, vol. 36, no. 8, pp. 22–31, 2021.

[6] Y. Su, Y. Liu, Y. Zhou, J. Yuan, H. Cao, and J. Shi, "Broadband LEO Satellite Communications: Architectures and Key Technologies," *IEEE Wireless Communications*, vol. 26, no. 2, pp. 55–61, 2019.

[7] M. R. Dakkak, D. G. Riviello, A. Guidotti, and A. Vanelli-Coralli, "Evaluation of multi-user multiple-input multiple-output digital beamforming algorithms in B5G/6G low Earth orbit satellite systems," *International Journal of Satellite Communications and Networking*, vol. n/a, no. n/a, 2023.

[8] K. N. R. S. V. Prasad, E. Hossain, and V. K. Bhargava, "Energy Efficiency in Massive MIMO-Based 5G Networks: Opportunities and Challenges," *IEEE Wireless Communications*, vol. 24, no. 3, pp. 86–94, 2017.

[9] G. Iacovelli, C. K. Sheemar, W. U. Khan, A. Mahmood, G. C. Alexandropoulos, J. Querol, and S. Chatzinotas, "Holographic MIMO for Next Generation Non-Terrestrial Networks: Motivation, Opportunities, and Challenges," *arXiv preprint arXiv:2411.10014*, 2024. Submitted on 15 Nov 2024.

[10] Z. Sun and Y. Jing, "Holographic MIMO NOMA Communications: A Power Saving Design," *IEEE Transactions on Wireless Communications*, vol. 23, no. 12, pp. 18711–18724, 2024.

[11] A. Zappone, B. Matthiesen, and A. Dekorsy, "Energy Efficiency of Holographic Transceivers Based on RIS," in *GLOBECOM 2022 - 2022 IEEE Global Communications Conference*, pp. 4613–4618, 2022.

[12] J. An, C. Yuen, C. Huang, M. Debbah, H. V. Poor, and L. Hanzo, "A Tutorial on Holographic MIMO Communications—Part III: Open Opportunities and Challenges," *IEEE Communications Letters*, vol. 27, no. 7, pp. 1674–1678, 2023.

[13] T. Gong, P. Gavriilidis, R. Ji, C. Huang, G. C. Alexandropoulos, L. Wei, Z. Zhang, M. Debbah, H. V. Poor, and C. Yuen, "Holographic MIMO Communications: Theoretical Foundations, Enabling Technologies, and Future Directions," *IEEE Communications Surveys & Tutorials*, pp. 1–1, 2023.

[14] Q. Li, M. Wen, and M. Di Renzo, "Single-RF MIMO: From Spatial Modulation to Metasurface-Based Modulation," *IEEE Wireless Communications*, vol. 28, no. 4, pp. 88–95, 2021.

[15] Q. Li, M. El-Hajjar, I. Hemadeh, A. Shojaeifard, A. A. M. Mourad, and L. Hanzo, "Reconfigurable Intelligent Surface Aided Amplitude- and Phase-Modulated Downlink Transmission," *IEEE Transactions on Vehicular Technology*, vol. 72, no. 6, pp. 8146–8151, 2023.

[16] Z. R. Omam, H. Taghvaee, A. Araghi, M. Garcia-Fernandez, G. Alvarez-Narciandi, G. C. Alexandropoulos, O. Yurduseven, and M. Khalily, "Holographic Metasurfaces Enabling Wave Computing for 6G: Status Overview, Challenges, and Future Research Trends," 2025.

[17] R. Deng, Y. Zhang, H. Zhang, B. Di, H. Zhang, H. V. Poor, and L. Song, "Reconfigurable Holographic Surfaces for Ultra-Massive MIMO in 6G: Practical Design, Optimization and Implementation," *IEEE Journal on Selected Areas in Communications*, vol. 41, no. 8, pp. 2367–2379, 2023.

[18] R. Deng, Y. Zhang, H. Zhang, B. Di, H. Zhang, and L. Song, "Reconfigurable Holographic Surface: A New Paradigm to Implement Holographic Radio," *IEEE Vehicular Technology Magazine*, vol. 18, no. 1, pp. 20–28, 2023.

[19] R. Deng, B. Di, H. Zhang, H. V. Poor, and L. Song, "Holographic MIMO for LEO Satellite Communications Aided by Reconfigurable Holographic Surfaces," *IEEE Journal on Selected Areas in Communications*, vol. 40, no. 10, pp. 3071–3085, 2022.

[20] J. An, C. Yuen, C. Huang, M. Debbah, H. V. Poor, and L. Hanzo, "A Tutorial on Holographic MIMO Communications—Part II: Performance Analysis and Holographic Beamforming," *IEEE Communications Letters*, vol. 27, no. 7, pp. 1669–1673, 2023.

[21] L. Sanguinetti, A. A. D'Amico, and M. Debbah, "Wavenumber-Division Multiplexing in Line-of-Sight Holographic MIMO Communications," *IEEE Transactions on Wireless Communications*, vol. 22, no. 4, pp. 2186–2201, 2023.

[22] L. Wei, C. Huang, G. C. Alexandropoulos, W. E. I. Sha, Z. Zhang, M. Debbah, and C. Yuen, "Multi-User Holographic MIMO Surfaces: Channel Modeling and Spectral Efficiency Analysis," *IEEE Journal of Selected Topics in Signal Processing*, vol. 16, no. 5, pp. 1112–1124, 2022.

[23] S. Zeng, H. Zhang, B. Di, H. Qin, X. Su, and L. Song, "Reconfigurable Refractive Surfaces: An Energy-Efficient Way to Holographic MIMO," *IEEE Communications Letters*, vol. 26, no. 10, pp. 2490–2494, 2022.

[24] J. Carlson, M. R. Castellanos, and R. W. Heath, "Hierarchical Codebook Design With Dynamic Metasurface Antennas for Energy-Efficient Arrays," *IEEE Transactions on Wireless Communications*, vol. 23, no. 10, pp. 14790–14804, 2024.

[25] X. Hu, R. Deng, B. Di, H. Zhang, and L. Song, "Holographic Beamforming for LEO Satellites," *IEEE Communications Letters*, vol. 27, no. 10, pp. 2717–2721, 2023.

[26] M. Johnson, S. Brunton, N. Kundtz, and N. Kutz, "Extremum-seeking control of the beam pattern of a reconfigurable holographic metamaterial antenna," *J Opt Soc Am A Opt Image Sci Vis*, vol. 33, no. 1, pp. 59–68, 2016.

[27] H. Zhang, N. Shlezinger, F. Guidi, D. Dardari, M. F. Imani, and Y. C. Eldar, "Beam Focusing for Near-Field Multiuser MIMO Communications," *IEEE Transactions on Wireless Communications*, vol. 21, no. 9, pp. 7476–7490, 2022.

[28] J. Xu, L. You, G. C. Alexandropoulos, X. Yi, W. Wang, and X. Gao, "Near-Field Wideband Extremely Large-scale MIMO Transmissions with Holographic Metasurface-Based Antenna Arrays," *IEEE Transactions on Wireless Communications*, pp. 1–1, 2024.

[29] E. Björnson, L. Sanguinetti, J. Hoydis, and M. Debbah, "Optimal Design of Energy-Efficient Multi-User MIMO Systems: Is Massive MIMO the Answer?," *IEEE Transactions on Wireless Communications*, vol. 14, no. 6, pp. 3059–3075, 2015.

[30] M. C. Johnson, S. L. Brunton, N. B. Kundtz, and J. N. Kutz, "Sidelobe Canceling for Reconfigurable Holographic Metamaterial Antenna," *IEEE Transactions on Antennas and Propagation*, vol. 63, no. 4, pp. 1881–1886, 2015.

[31] A. Araghi, M. Khalily, P. Xiao, and R. Tafazolli, "Holographic-Based Leaky-Wave Structures: Transformation of Guided Waves to Leaky Waves," *IEEE Microwave Magazine*, vol. 22, no. 6, pp. 49–63, 2021.

[32] R. Deng, B. Di, H. Zhang, Y. Tan, and L. Song, "Reconfigurable Holographic Surface: Holographic Beamforming for Metasurface-Aided Wireless Communications," *IEEE Transactions on Vehicular Technology*, vol. 70, no. 6, pp. 6255–6259, 2021.

[33] N. Shlezinger, G. C. Alexandropoulos, M. F. Imani, Y. C. Eldar, and D. R. Smith, "Dynamic Metasurface Antennas for 6G Extreme Massive MIMO Communications," *IEEE Wireless Communications*, vol. 28, no. 2, pp. 106–113, 2021.

[34] A. E. Matemu and K. Lee, "Spatial modulation and generalized spatial modulation for dynamic metasurface antennas," *IEEE Transactions on Wireless Communications*, vol. 24, no. 1, pp. 783–795, 2025.

[35] 3rd Generation Partnership Project (3GPP), "Technical Report 38.811: Study on New Radio (NR) to support non-terrestrial networks," Tech. Rep. 38.811, 3GPP, 2021.

[36] G. Torcolacci, N. Decarli, and D. Dardari, "Holographic MIMO Communications Exploiting the Orbital Angular Momentum," *IEEE Open Journal of the Communications Society*, vol. 4, pp. 1452–1469, 2023.

[37] D. R. Smith, O. Yurduseven, L. P. Mancera, P. Bowen, and N. B. Kundtz, "Analysis of a Waveguide-Fed Metasurface Antenna," *Phys. Rev. Appl.*, vol. 8, p. 054048, Nov 2017.

[38] H. Chen, S. Zeng, H. Guo, T. Svensson, and H. Zhang, "Near-Far Field Channel Modeling for Holographic MIMO Using Expectation-Maximization Methods," in *2024 IEEE Wireless Communications and Networking Conference (WCNC)*, pp. 1–6, 2024.

[39] Q. Li, M. El-Hajjar, K. Cao, C. Xu, H. Haas, and L. Hanzo, "Holographic Metasurface-Based Beamforming for Multi-Altitude LEO Satellite Networks," *IEEE Transactions on Wireless Communications*, vol. 24, no. 4, pp. 3103–3116, 2025.

[40] T. Gong, L. Wei, C. Huang, G. C. Alexandropoulos, M. Debbah, and C. Yuen, "Near-field channel modeling for holographic mimo communications," *IEEE Wireless Communications*, vol. 31, no. 3, pp. 108–116, 2024.

[41] A. Enqvist, Özlem Tuğfe Demir, C. Cavdar, and E. Björnson, "Fundamentals of Energy-Efficient Wireless Links: Optimal Ratios and Scaling Behaviors," 2024.

[42] M. R. Castellanos, S. Yang, C.-B. Chae, and R. W. Heath Jr, "Embracing Reconfigurable Antennas in the Tri-hybrid MIMO Architecture for 6G," *arXiv preprint arXiv:2501.16610*, 2025. IEEE Transactions on Communications (invited).

[43] L. You, X. Qiang, K.-X. Li, C. G. Tsinos, W. Wang, X. Gao, and B. Ottersten, "Massive MIMO Hybrid Precoding for LEO Satellite Communications With Twin-Resolution Phase Shifters and Nonlinear Power Amplifiers," *IEEE Transactions on Communications*, vol. 70, no. 8, pp. 5543–5557, 2022.

[44] Y. Liu, C. Li, J. Li, and L. Feng, "Robust Energy-Efficient Hybrid Beamforming Design for Massive MIMO LEO Satellite Communication Systems," *IEEE Access*, vol. 10, pp. 63085–63099, 2022.

[45] J. Palacios, N. González-Prelcic, C. Mosquera, T. Shimizu, and C.-H. Wang, "A Hybrid Beamforming Design for Massive MIMO LEO Satellite Communications," *Frontiers in Space Technologies*, vol. Volume 2 - 2021, 2021.

[46] L. N. Ribeiro, S. Schwarz, M. Rupp, and A. L. F. de Almeida, "Energy Efficiency of mmWave Massive MIMO Precoding With Low-Resolution DACs," *IEEE Journal of Selected Topics in Signal Processing*, vol. 12, no. 2, pp. 298–312, 2018.